Article ID: 1001-3555(2015)06-0553-10

Catalytic Decomposition of N_2O over $Ce_xCo_{2-x}AlO_4$ Composite Oxides Prepared by Sol-gel Method

WANG Jian, WU Cang-cang, ZHENG Li, XU Xiu-feng*
(*Institute of Applied Catalysis, Yantai University, Yantai* 264005, *China*)

Abstract: A series of $Ce_xCo_{2-x}AlO_4$ composite oxides were prepared by citric acid based sol-gel method and further modified by K_2CO_3. The effect of composite oxide compositions, pH values of mother liquid, and potassium loadings on catalytic activity for N_2O decomposition was investigated. The bare and K-modified $Ce_xCo_{2-x}AlO_4$ catalysts were characterized by means of nitrogen physisorption, X-ray diffraction(XRD), scanning electron microscopy(SEM), hydrogen temperature-programmed reduction(H_2-TPR), temperature-programmed desorption of oxygen(O_2-TPD), and X-ray photoelectron spectroscopy(XPS) techniques. The results show that the catalytic activity of $Ce_xCo_{2-x}AlO_4$ composite oxides was enhanced in comparison with Co_2AlO_4, and the optimal composition was $Ce_{0.05}Co_{1.95}AlO_4$ with larger surface area, smaller particle size and the Ce-Co synergistic effect. Further results indicate that 0.05 K/$Ce_{0.05}Co_{1.95}AlO_4$ catalyst due to the electronic effect of potassium on cobalt oxides was more active than other catalysts, over which N_2O conversion reached 98.5% at 450 ℃ after 50 h continuous reaction in the presence of oxygen.

Key words: catalytic decomposition of N_2O; $Ce_xCo_{2-x}AlO_4$ composite oxides; sol-gel method; K-modified catalysts
CLC number: O643.3 **Document code**: A

Anthropogenic N_2O mainly emits from some industrial processes such as nitric acid production. N_2O has high global warming potential (GWP) of 310 and long lifetime of 120 years in atmosphere, furthermore N_2O contributes to the destruction of ozone layer in the stratosphere. Therefore, N_2O was listed in the six most noticeable greenhouse gases controlled by Kyoto protocol. Catalytic decomposition of N_2O into nitrogen and oxygen has been considered as an economic method to destruct this harmful gas. So far, catalysts including supported noble metals[1-4], ion-exchanged zeolites[5-7], and transition metal oxides[8-10] have been used for N_2O decomposition. Among these catalysts, transition metal oxides especially cobalt-based spinel oxides have attracted much attention.

In our previous work, we reported that the substitution of partial Co in cobalt-based catalysts by Ni[11] or Mn[12] improved the catalytic activity and stability. Xue[13-14] and Dziembaj[15] reported that the addition of CeO_2 to Co_3O_4 could improve the reduction of Co^{3+} to Co^{2+} and then promote the N_2O decomposition; furthermore, the activity of Ce-Co mixed oxides in N_2O decomposition could be enhanced significantly through modifying with K[16-17].

In this work, a series of $Ce_xCo_{2-x}AlO_4$ composite oxides were prepared by sol-gel method and impregnated by K_2CO_3 solution. The effect of catalyst compositions, pH values of mother liquid, and potassium loadings on catalytic activity for N_2O decomposition was investigated. In addition, the catalysts stability in atmosphere of oxygen-alone or oxygen-steam together was tested.

1 Experimental

1.1 Catalyst preparation

1.1.1 $Ce_xCo_{2-x}AlO_4$ with different compositions

$Ce_xCo_{2-x}AlO_4$ composite oxides were prepared by sol-gel method with citric acid as chelating agent. 1 mol/L

Received date: 2015-09-26; **Revised date**: 2015-10-20.
Foundation: This work was supported by the Department of Science and Technology of Shandong Province (No. 2012GSF11708) and Graduate Innovation Foundation of Yantai University (GIFYTU).
First author: Wang Jian (1990-), Male, Master candidate.
* **Corresponding author**: Xu Xiu-feng, Tel.: 0535-6902746, E-mail: xxf@ytu.edu.cn.

citric acid solution was dropped into the same volume aqueous solution containing stoichiometric amounts of $Ce(NO_3)_3$, $Co(NO_3)_2$ and $Al(NO_3)_3$ with a total cation concentration of 1 mol/L. The mixed solution with pH value of 0.5 was vigorously stirred at room temperature for 30 min. Then the solution was concentrated by a rotary evaporator at 65 ℃ to reach a viscous state, dried at 120 ℃ for 12 h to gain xerogel, and calcined at 600 ℃ for 4 h. The as-prepared catalysts were denoted as $Ce_xCo_{2-x}AlO_4$ (x = 0, 0.03, 0.05, 0.10, 0.15, 0.20).

1.1.2 $Ce_{0.05}Co_{1.95}AlO_4$ with different mother liquid pH values 1 mol/L citric acid solution was dropped into the same volume aqueous solution containing $Ce(NO_3)_3$, $Co(NO_3)_2$ and $Al(NO_3)_3$ with a total cation concentration of 1 mol/L and Ce/Co/Al atomic ratio of 0.05/1.95/1. The pH value of above mixed solution was adjusted to a required value by 2.5% ammonia solution. The as-prepared catalysts were denoted as $Ce_{0.05}Co_{1.95}AlO_4$(pH=y), where y is the value of mother liquid in the range of 0.5 ~ 5.

1.1.3 K_2CO_3 modified $Ce_{0.05}Co_{1.95}AlO_4$(pH=2) catalysts $Ce_{0.05}Co_{1.95}AlO_4$(pH=2) was incipiently impregnated by K_2CO_3 solution at room temperature for 24 h, dried at 120 ℃ for 12 h, and calcined at 600 ℃ for 4 h. The catalysts were denoted as zK/$Ce_{0.05}Co_{1.95}AlO_4$(pH=2), where z refers to the molar ratio of K/(Ce+Co) in the range of 0.03 ~ 0.10.

1.2 N_2O decomposition reaction

N_2O decomposition was carried out in a fixed-bed reactor using 1 g catalyst (particle size 0.45 ~ 0.28 mm). Unless otherwise stated, the feed gases consisted of 2% N_2O and 4% O_2 balanced in argon at a total flow rate of 140 mL/min. For the catalytic activity and stability test in steam-oxygen together, the feed gases were 2% N_2O, 4% O_2, 8.8% H_2O and argon.

The outlet gases were analyzed with a gas chromatography (GC-920, Shanghai Haixin) equipped with Porapak Q column and thermal conductivity detector (TCD). N_2O conversion was calculated at each temperature for 30 min after reaction.

In catalytic stability test, the temperature was raised from room temperature to 450 ℃ with a ramping rate of 10 ℃/min, kept at 450 ℃ for 50 h, and N_2O conversion was measured every 2 h.

1.3 Catalyst characterization

BET surface area of catalysts was measured by nitrogen physisorption using an automated adsorption apparatus (NOVA3000, Quantachrome). Prior to the measurement, the samples were pretreated at 300 ℃ for 3 h under vacuum to remove any impurities.

The catalysts phases were characterized by X-ray diffraction (XRD) on a powder X-ray diffractometer (XRD-6100, Shimadzu) with CuKα radiation and graphite monochromator, operating at 40 kV and 30 mA. The crystallite size of crystallographic plane (311) attributed to spinel-structure catalyst was measured by Scherrer equation:

$$D = \frac{0.89\lambda}{\beta \cdot \cos\theta}$$

where β is the FWHM of diffraction peak and θ is the diffraction angle.

Temperature programmed reduction of hydrogen (H_2-TPR) and temperature programmed desorption of oxygen(O_2-TPD) were performed using an adsorption apparatus (PCA-1200, Beijing Builder). Prior to the H_2-TPR measurement, 80 mg catalyst was pretreated under Ar flow at 500 ℃ for 30 min. After cooling down to ambient temperature, the catalyst was heated from room temperature to 900 ℃ under 10% H_2/Ar flow at a ramping rate of 10 ℃/min, and the hydrogen consumption was monitored by TCD. Before O_2-TPD measurement, 100 mg catalyst was pretreated under pure O_2 at 120 ℃ for 30 min. After cooling to ambient temperature and getting a smooth baseline, the catalyst was heated from room temperature to 900 ℃ under pure He flow at a ramping rate of 10 ℃/min, and the oxygen desorption was measured by TCD.

The morphology of catalysts was observed with a scanning electron microscopy (SEM, S-4800, Hitachi). To improve the electric conductivity, the catalyst sample was coated previously with platinum by using an ion sputter (E-1045, Hitachi).

X-ray photoelectron spectra (XPS) of cobalt and cerium elements on catalyst surface were recorded in an ESCALAB250 spectrometer using Al $K\alpha$ radiation with

pass energy of 20 eV. The charging effect was corrected by referencing C 1s peak centered at 284.6 eV.

2 Results and discussion

2.1 Catalytic activity of $Ce_xCo_{2-x}AlO_4$ composite oxides with different compositions

XRD patterns of $Ce_xCo_{2-x}AlO_4$ composite oxides are shown in Figure 1. The dominant peaks of all the catalysts are ascribed to (220), (311), (400), (422), and (511) crystallographic planes indexed to spinel-structure phases. In addition, a small peak ascribed to CeO_2 appeared in $Ce_{0.15}Co_{1.85}AlO_4$ and $Ce_{0.20}Co_{1.80}AlO_4$ catalysts. It is demonstrated that the ceria existed as highly dispersed or amorphous species in $Ce_{0.03}Co_{1.97}AlO_4$ and $Ce_{0.05}Co_{1.95}AlO_4$ catalysts, resembling with the results reported by Xue[13-14].

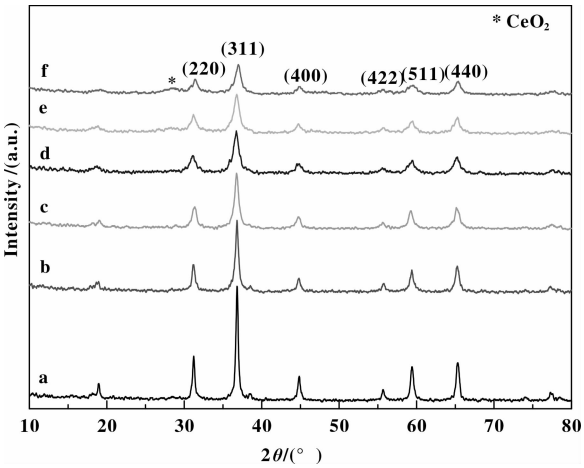

Fig. 1 XRD patterns of $Ce_xCo_{2-x}AlO_4$ with different compositions

a. Co_2AlO_4; b. $Ce_{0.03}Co_{1.97}AlO_4$; c. $Ce_{0.05}Co_{1.95}AlO_4$; d. $Ce_{0.10}Co_{1.90}AlO_4$; e. $Ce_{0.15}Co_{1.85}AlO_4$; f. $Ce_{0.20}Co_{1.80}AlO_4$

Figure 2 presents the N_2O conversions over $Ce_xCo_{2-x}AlO_4$ with different compositions. We can see the catalysts with Ce substitution for Co exhibited higher activity than Co_2AlO_4. The catalytic activity was improved to a maximum value at $x = 0.05$ in $Ce_xCo_{2-x}AlO_4$, then decreased with increase in Ce contents. The $Ce_{0.05}Co_{1.95}AlO_4$ catalyst exhibited better activity than other catalysts. BET surface area and crystallite sizes of $Ce_xCo_{2-x}AlO_4$ are listed in Table 1. It can be seen that the crystallite size decreased gradually with the increasing content of Ce, thus the XRD peaks intensity was weakened, while the BET surface area presented irregularly.

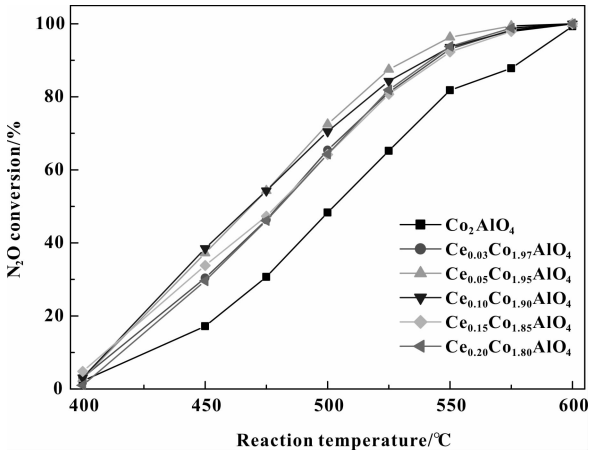

Fig. 2 N_2O conversions over $Ce_xCo_{2-x}AlO_4$ with different compositions

Table 1 BET surface area and crystallite size of $Ce_xCo_{2-x}AlO_4$ with different compositions

Catalysts	Crystallite size[a] /nm	BET surface area /($m^2 \cdot g^{-1}$)
Co_2AlO_4	37.7	46.3
$Ce_{0.03}Co_{1.97}AlO_4$	31.6	30.5
$Ce_{0.05}Co_{1.95}AlO_4$	22.3	39.0
$Ce_{0.10}Co_{1.90}AlO_4$	16.0	47.7
$Ce_{0.15}Co_{1.85}AlO_4$	12.1	50.4
$Ce_{0.20}Co_{1.80}AlO_4$	13.0	50.1

a. Calculated by Scherrer equation on the basis of (311) crystallographic plane data in XRD patterns.

N_2O decomposition mechanism can be described as follows[8]. N_2O molecule is adsorbed on catalyst active sites, resulting in the weakening and breaking of N—O bond, followed by the production of N_2 and surface oxygen atom, then the surface oxygen atoms react with each other to form oxygen molecule and desorb from catalysts surface. In this process, the desorption of surface oxygen atoms is a controlling step. Figure 3 shows the H_2-TPR profiles of $Ce_xCo_{2-x}AlO_4$ catalysts. It was reported that the reduction temperatures of surface and bulk CeO_2 were ca. 540 and 840 ℃, respectively[18]. As shown in Figure 3, the low temperature peak at 350 ~540 ℃ is ascribed to the mixed reduc-

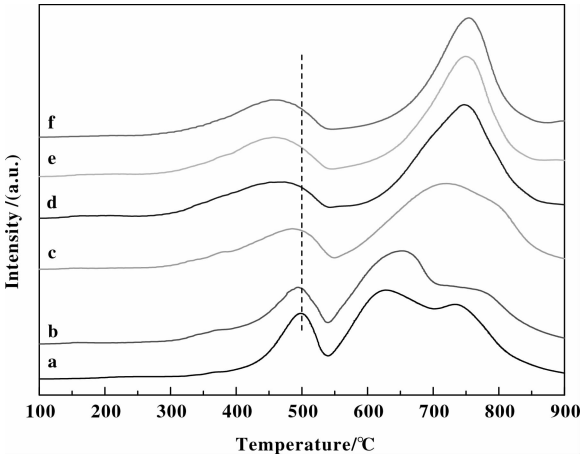

Fig. 3 H_2-TPR profiles of $Ce_xCo_{2-x}AlO_4$ with different compositions

a. Co_2AlO_4; b. $Ce_{0.03}Co_{1.97}AlO_4$; c. $Ce_{0.05}Co_{1.95}AlO_4$; d. $Ce_{0.10}Co_{1.90}AlO_4$; e. $Ce_{0.15}Co_{1.85}AlO_4$; f. $Ce_{0.20}Co_{1.80}AlO_4$

tion of Co^{3+} to Co^{2+} and surface CeO_2 to Ce_2O_3, while the high temperature at 540 ~850 ℃ can be assigned to reduction of Co^{2+} to Co^0 and bulk CeO_2 to Ce_2O_3. It can be seen the reduction temperature of CeO_2 shifted to lower temperature due to the effect of cobalt. Considering the actual reaction temperature, the catalytic activity is just associated with the reduction peak below 600 ℃. We found that the reduction temperature of Co^{3+} to Co^{2+} lowered gradually with increasing Ce, indicating that the oxygen atom bonded with cobalt ion was easily removed, that is, the oxygen migration was promoted and N_2O decomposition was enhanced. It is indicated that the good reducibility of cobalt and cerium ions due to their synergistic effect in Ce-Co catalysts is a crucial factor for their excellent performance.

2.2 Catalytic activity of $Ce_{0.05}Co_{1.95}AlO_4$ composite oxides prepared by mother liquids with different pH values

The XRD patterns of $Ce_{0.05}Co_{1.95}AlO_4$ with different pH values of mother liquid are shown in Figure 4, and the peaks ascribed to (220), (311), (400), (422), and (511) crystallographic planes in spinel-structure phases are observed, indicating that the difference of mother liquid pH values has not changed the catalysts structure. The particle morphology of $Ce_{0.05}Co_{1.95}AlO_4$ catalysts is given in Figure 5. It can be seen that $Ce_{0.05}Co_{1.95}AlO_4$ (pH = 2) revealed the minimal particles, in addition, the space between particles became broader as pH values increased. It is thought that the chelating degree of metallic ions and the particle morphology may be affected by chemical forms of citric acid at different pH values.

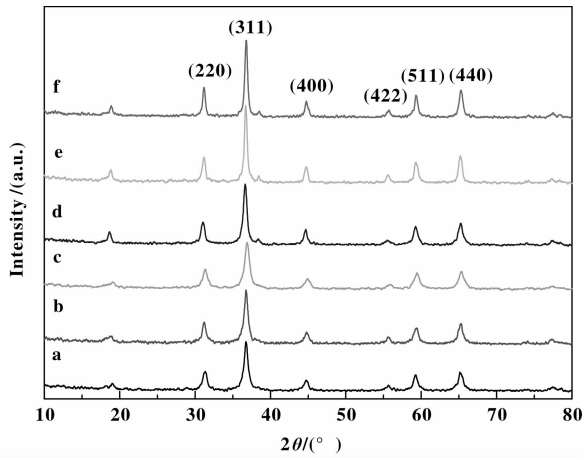

Fig. 4 XRD patterns of $Ce_{0.05}Co_{1.95}AlO_4$ with different pH values of mother liquid

a. pH=0.5; b. pH=1; c. pH=2; d. pH=3; e. pH=4; f. pH=5

Figure 6 illustrates that the activity of $Ce_{0.05}Co_{1.95}AlO_4$ is related to the pH value of mother liquid, and a maximum N_2O conversion is achieved over the $Ce_{0.05}Co_{1.95}AlO_4$ prepared with a pH value of 2. Table 2 lists the BET surface area and crystallite size of $Ce_{0.05}Co_{1.95}AlO_4$. The catalyst with pH value of 2 has the largest surface area and smallest crystallite, which is relevant to its superior performance.

H_2-TPR profiles of $Ce_{0.05}Co_{1.95}AlO_4$ are shown in Figure 7. The $Ce_{0.05}Co_{1.95}AlO_4$ (pH = 2) catalyst exhibited easier reduction of Co^{3+} to Co^{2+} than others, thus the oxygen species was desorbed easily and catalytic activity was improved. In order to further elucidate the influencing factors for catalysts activity, O_2-TPD profiles were measured and shown in Figure 8. Several peaks of desorbed oxygen species can be ascribed to the desorption of surface adsorbed oxygen. It is reported that the amount of oxygen desorption was associated with catalyst activity, *i. e.*, catalyst with higher activity adsorbed larger amount of oxygen species[19-21]. As shown in Figure 8, the desorbed oxygen

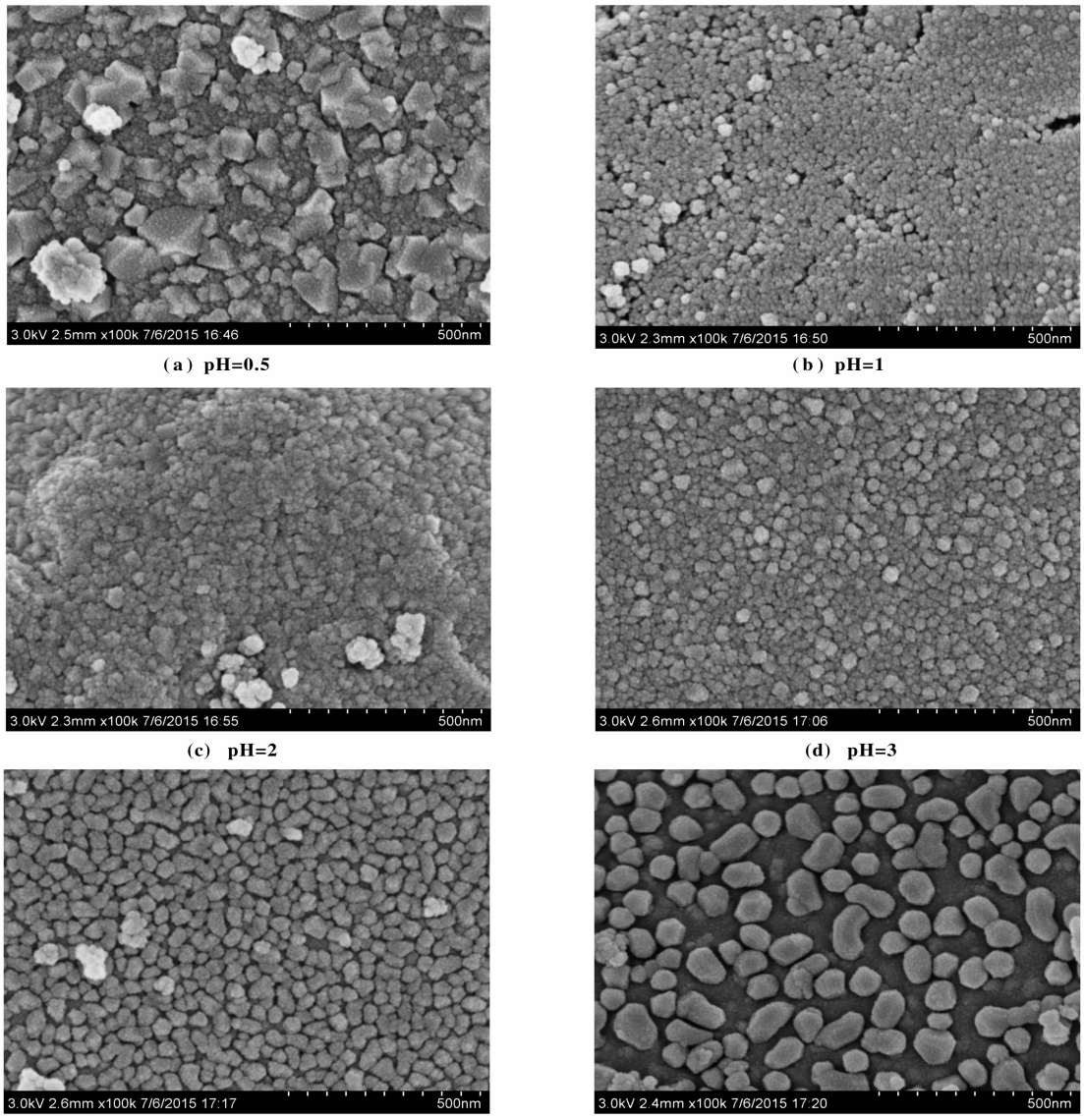

Fig. 5 SEM images of $Ce_{0.05}Co_{1.95}AlO_4$ with different pH values of mother liquid

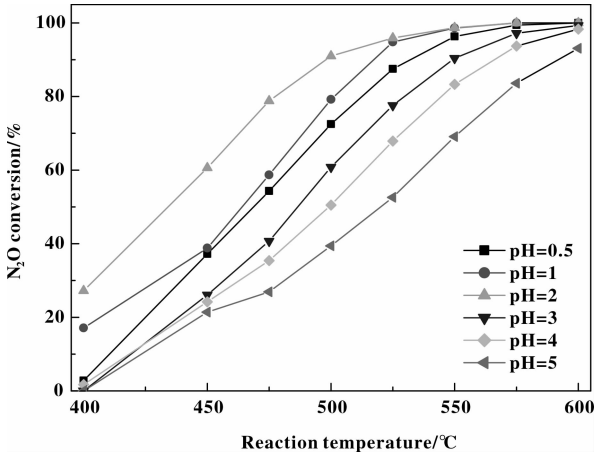

Fig. 6 N_2O conversions over $Ce_{0.05}Co_{1.95}AlO_4$ with different pH values of mother liquid

Table 2 BET surface area and crystallite size of $Ce_{0.05}Co_{1.95}AlO_4$ with different pH values of mother liquid

Catalysts	Crystallite size[a]/nm	BET surface area /($m^2 \cdot g^{-1}$)
$Ce_{0.05}Co_{1.95}AlO_4$(pH=0.5)	22.3	39.0
$Ce_{0.05}Co_{1.95}AlO_4$(pH=1)	18.7	46.8
$Ce_{0.05}Co_{1.95}AlO_4$(pH=2)	12.5	69.9
$Ce_{0.05}Co_{1.95}AlO_4$(pH=3)	21.8	52.0
$Ce_{0.05}Co_{1.95}AlO_4$(pH=4)	28.8	42.8
$Ce_{0.05}Co_{1.95}AlO_4$(pH=5)	24.3	38.2

a. Calculated by Scherrer equation on the basis of (311) crystallographic plane data in XRD patterns.

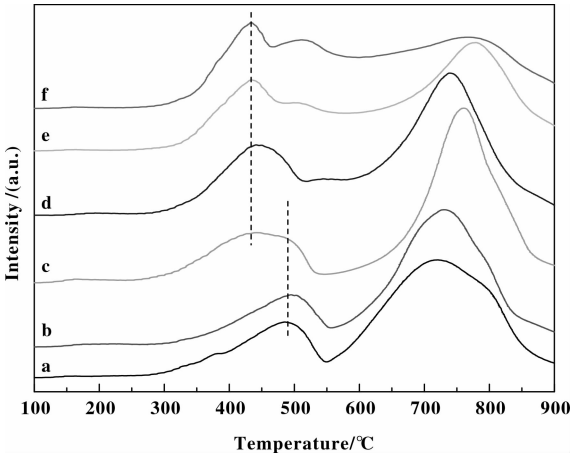

Fig. 7 H_2-TPR profiles of $Ce_{0.05}Co_{1.95}AlO_4$ with different pH values of mother liquid
a. pH=0.5; b. pH=1; c. pH=2; d. pH=3; e. pH=4; f. pH=5

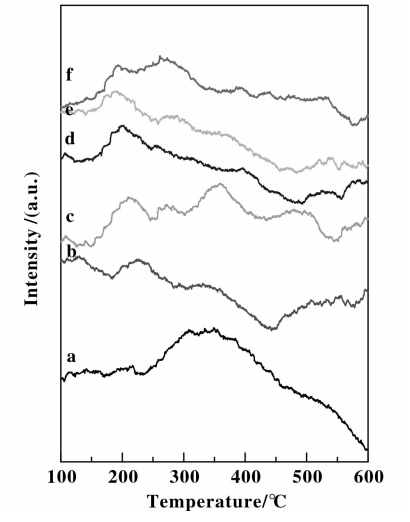

Fig. 8 O_2-TPD profiles of $Ce_{0.05}Co_{1.95}AlO_4$ with different pH values of mother liquid
a. pH=0.5; b. pH=1; c. pH=2; d. pH=3; e. pH=4; f. pH=5

amount from $Ce_{0.05}Co_{1.95}AlO_4$(pH=2) was more than other catalysts, indicating the larger amount of adsorbed oxygen and lower desorption temperature was contributed to the superior performance of $Ce_{0.05}Co_{1.95}AlO_4$(pH=2).

2.3 Catalytic activity of K-modified $Ce_{0.05}Co_{1.95}AlO_4$(pH=2) catalysts

In this part, the optimal catalyst $Ce_{0.05}Co_{1.95}AlO_4$ (pH=2) was modified by potassium. As shown in Figure 9, K-modified catalysts were spinel-structure without any impurities. Table 3 lists the BET surface area and crystallite size of $K/Ce_{0.05}Co_{1.95}AlO_4$(pH=2) catalysts. It is shown that the BET surface area tended to a slight decrease with the increase in potassium loadings, while the crystallite size was similar.

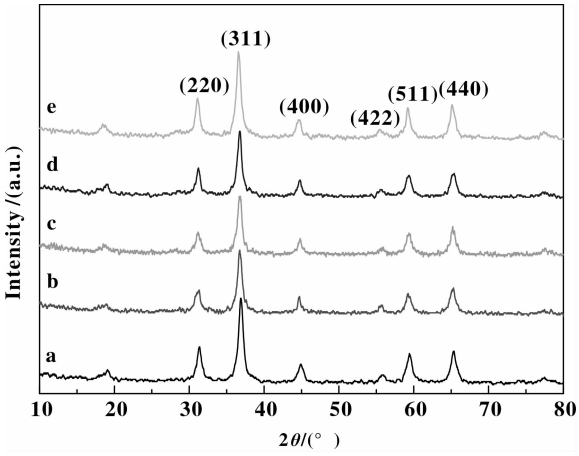

Fig. 9 XRD patterns of $K/Ce_{0.05}Co_{1.95}AlO_4$(pH=2) with different potassium loadings
a. $Ce_{0.05}Co_{1.95}AlO_4$; b. $0.03K/Ce_{0.05}Co_{1.95}AlO_4$; c. $0.05K/Ce_{0.05}Co_{1.95}AlO_4$; d. $0.08K/Ce_{0.05}Co_{1.95}AlO_4$; e. $0.10K/Ce_{0.05}Co_{1.95}AlO_4$

Table 3 BET surface area and crystallite size of $K/Ce_{0.05}Co_{1.95}AlO_4$(pH=2) with different potassium loadings

Catalysts	Crystallite size[a] /nm	BET surface area /($m^2 \cdot g^{-1}$)
$Ce_{0.05}Co_{1.95}AlO_4$	12.5	69.9
$0.03K/Ce_{0.05}Co_{1.95}AlO_4$	13.1	59.4
$0.05K/Ce_{0.05}Co_{1.95}AlO_4$	15.1	57.1
$0.08K/Ce_{0.05}Co_{1.95}AlO_4$	12.3	57.5
$0.10K/Ce_{0.05}Co_{1.95}AlO_4$	19.2	50.9

a. Calculated by Scherrer equation on the basis of (311) crystallographic plane data in XRD patterns.

Figure 10 presents the N_2O conversion on $K/Ce_{0.05}Co_{1.95}AlO_4$ catalysts, 0.05 $K/Ce_{0.05}Co_{1.95}AlO_4$ (pH=2) catalyst exhibited higher activity than other catalysts for N_2O decomposition. As shown in Figure 11, the reduction peaks ascribed to Co^{3+} to Co^{2+} and surface CeO_2 to Ce_2O_3 tended to lower temperature with

the increase in potassium loadings, in response to their better catalytic activity, followed by a decrease in catalytic activity because some active sites on catalysts surface were coated by excessive potassium. We suggest that the appropriate potassium loadings and good reduction of Co^{3+}-O^- in catalysts play an important role on superior performance for N_2O decomposition.

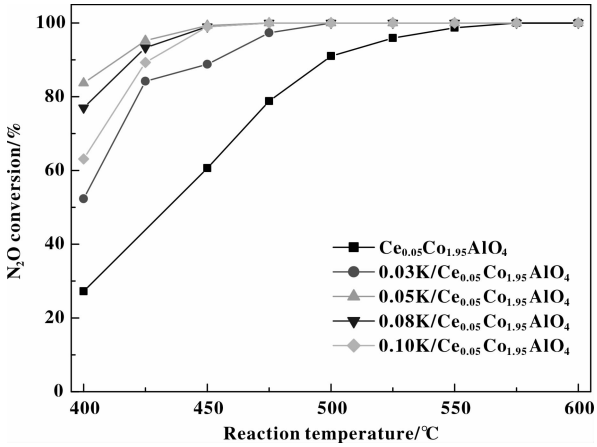

Fig. 10 N_2O conversions of $K/Ce_{0.05}Co_{1.95}AlO_4$ (pH=2) with different potassium loadings

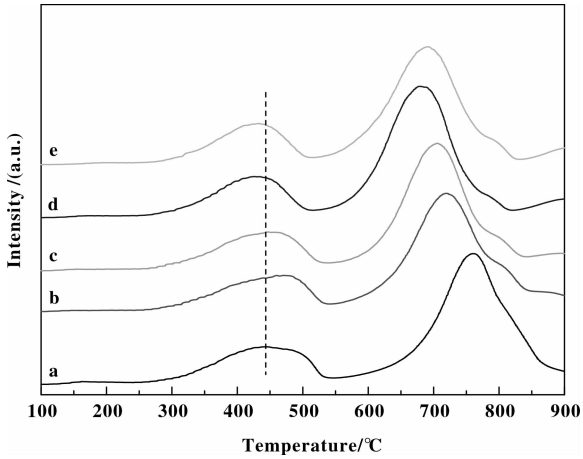

Fig. 11 H_2-TPR profiles of $K/Ce_{0.05}Co_{1.95}AlO_4$ (pH=2) with different potassium loadings

a. $Ce_{0.05}Co_{1.95}AlO_4$; b. $0.03K/Ce_{0.05}Co_{1.95}AlO_4$; c. $0.05K/Ce_{0.05}Co_{1.95}AlO_4$; d. $0.08K/Ce_{0.05}Co_{1.95}AlO_4$; e. $0.10K/Ce_{0.05}Co_{1.95}AlO_4$

Figure 12 shows the XPS spectra of cobalt and cerium elements on the surface of $Ce_{0.05}Co_{1.95}AlO_4$ and $K/Ce_{0.05}Co_{1.95}AlO_4$ catalysts. In Figure 12 (A), the binding energy (BE) of Co $2p_{3/2}$ in $K/Ce_{0.05}Co_{1.95}AlO_4$

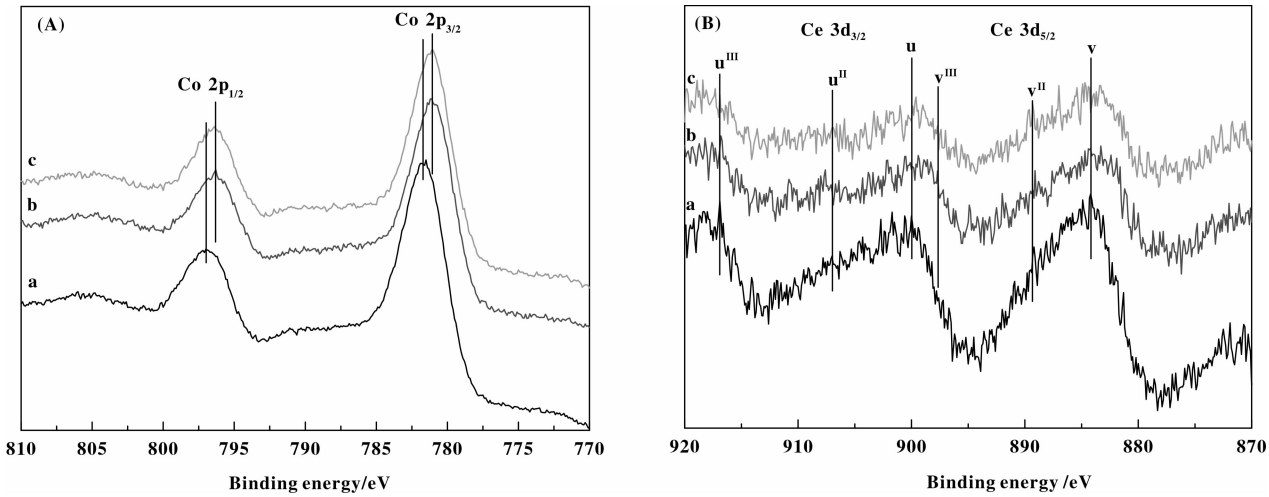

Fig. 12 XPS spectra of cobalt and cerium on the surface of $K/Ce_{0.05}Co_{1.95}AlO_4$ (pH=2)

a. $Ce_{0.05}Co_{1.95}AlO_4$; b. $0.05K/Ce_{0.05}Co_{1.95}AlO_4$; c. $0.10K/Ce_{0.05}Co_{1.95}AlO_4$

catalysts shifted to a lower value of 0.3 eV compared with un-doped catalyst. We suggest that the electronic effect of potassium resulted in the change of chemical environments of Co ions and thus the improved catalytic activity of K-modified catalysts. Figure 12 (B) shows the XPS spectra of Ce 3d ions, no great difference in BE of Ce 3d between K-doped and un-doped catalysts can be found. It is thought that the promotional effect of K on cobalt oxides was more significant than ceria. Similar result was reported in K-doped Co-Ce mixed oxides[16]. In sum, K-modified catalysts presented good reduction of Co^{3+}-O^- to Co^{2+} due to the electronic

effect of potassium on cobalt oxides, and thus high catalytic activity.

2.4 Catalytic activity and stability of K/$Ce_{0.05}Co_{1.95}AlO_4$ (pH = 2) in oxygen and steam

Catalytic activity and stability of K/$Ce_{0.05}Co_{1.95}AlO_4$(pH=2) catalyst are tested under various atmospheres and N_2O conversions are shown in Figures 13-14. It is found that the activity and stability in the presence of steam was declined due to the occupation

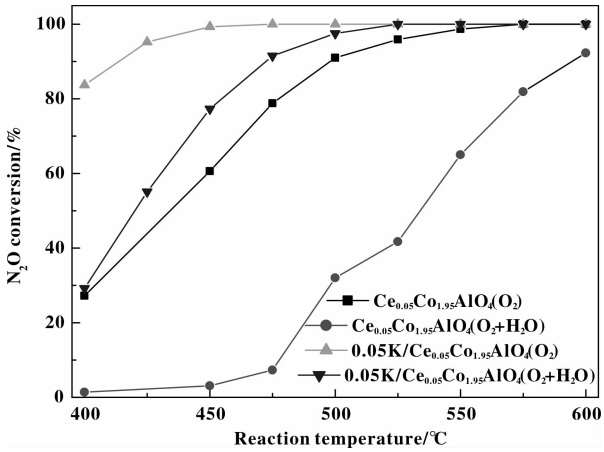

Fig. 13 N_2O conversions over K-promoted $Ce_{0.05}Co_{1.95}AlO_4$ catalysts under various atmospheres

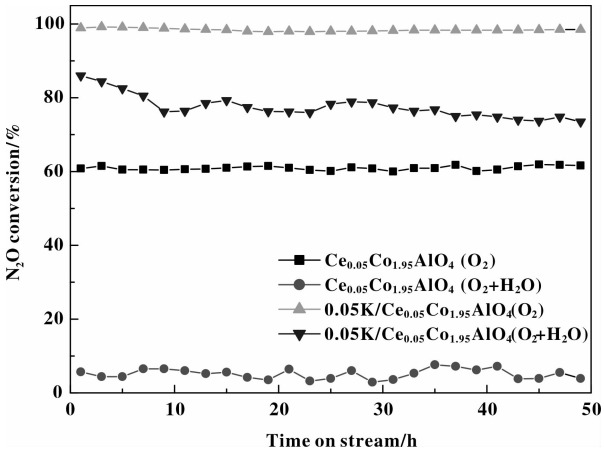

Fig. 14 Stability of K-promoted $Ce_{0.05}Co_{1.95}AlO_4$ catalysts under various atmospheres at 450 ℃

of water molecule on catalysts surface. After continuous reaction at 450 ℃ for 50 h, N_2O conversion over 0.05 K/$Ce_{0.05}Co_{1.95}AlO_4$(pH=2) kept 98.5% and 73.5% in oxygen-alone and oxygen-steam together, respectively, while that on un-doped $Ce_{0.05}Co_{1.95}AlO_4$ (pH=2) was only 61.6% and 3.9%. As a contrast, 0.05 K/$Ce_{0.05}Co_{1.95}AlO_4$(pH=2) exhibited a better catalytic performance than un-modified catalyst.

3 Conclusions

$Ce_xCo_{2-x}AlO_4$ composite oxides were prepared by sol-gel method with citric acid as chelating agent and further modified by K_2CO_3. The composite oxide compositions, pH values of mother liquid and potassium loadings produced significant effect on catalysts activity for N_2O decomposition. The results show that 0.05 K/$Ce_{0.05}Co_{1.95}AlO_4$(pH=2) is an active catalyst, over which N_2O conversion reached 98.5% and 73.5% at 450 ℃ after 50 h runs in the atmosphere of oxygen-alone and oxygen-steam together, respectively. In contrast to bare $Ce_xCo_{2-x}AlO_4$, K-modified catalysts presented higher catalytic activity and resistance against oxygen and water due to the electronic effect of K on cobalt oxides.

References:

[1] a. Kim S S, Lee S J, Hong S C. Effect of addition CeO_2 to Rh/Al_2O_3 catalyst on N_2O decomposition[J]. *Chem Eng J*, 2011, **169**(1/3): 173-179.

b. Zong Yue(宗 玥), Li Meng-li(李孟丽), Yang Xiao-long(杨晓龙), *et al.* Ru supported on foamed aluminum applied in the low-temperature catalytic decomposition of N_2O(泡沫铝负载钌基催化剂应用于 N_2O 的低温催化分解研究)[J]. *J Mol Catal(China)*(分子催化), 2014, **28**(4): 336-343.

c. Wang Jian(王 建), Zhang Hai-jie(张海杰), Xu Xiu-fen(徐秀峰). Catalytic decomposition of N_2O over $Cu_xFe_{1-x}Fe_2O_4$ and $Ni_xFe_{1-x}Fe_2O_4$ composite oxides(N_2O 在 $Cu_xFe_{1-x}Fe_2O_4$和 $Ni_xFe_{1-x}Fe_2O_4$复合氧化物催化剂上的分解反应)[J]. *J Mol Catal(China)*(分子催化), 2015, **29**(1): 75-81.

d. Wang Jian(王 建), Dou Zhe(窦 喆), Pan Yan-fei(潘燕飞), *et al.* Catalytic decomposition of N_2O over $Mn_xCo_{3-x}O_4$ mixed oxides and modified catalysts($Mn_xCo_{3-x}O_4$ 复合氧化物及改性催化剂催化分解 N_2O)[J]. *J Mol Catal(China)*(分子催化), 2015, **29**(3): 246-255.

[2] a. Hussain M, Akhter P, Fino D, *et al.* Modified KIT-6 and SBA-15-spherical supported metal catalysts for N_2O

decomposition[J]. *J Environ Chem Eng*, 2013, **1**(3): 164-174.

b. Feng Yu(封 煜), Liu Xin-yong(刘新勇), Jiang Zhi(江 治), *et al.* Photocatalysis activity of Pt/TiO_2 toward low concentration NO abatement(TiO_2 负载 Pt 对光催化去除低浓度 NO 性能的影响)[J]. *J Mol Catal(China)*(分子催化), 2013, **27**(1): 76-82.

c. Yu Hua-liang(俞华良), Chen Ming-xia(陈铭夏), Zou Gu-chu(邹谷初), *et al.* Simultaneously catalytic removal of diesel particulates and NO_x on K/$LiCoO_2$ catalysts(K/$LiCoO_2$ 的制备及其同时催化去除碳烟和 NO_x 的性能研究)[J]. *J Mol Catal(China)*(分子催化), 2013, **27**(1): 49-54.

d. Li Hui-juan(李惠娟), Jiang Xiao-yuan(蒋晓原), Zheng Xiao-ming(郑小明). Non-thermal-plasmacombined with selective catalytic reaction of NO by CH_4 over CuO/CeO_2-TiO_2/γ-Al_2O_3 catalyst(介质阻挡等离子体放电辅助 CuO/CeO_2-TiO_2/γ-Al_2O_3 催化剂脱除 NO 的研究)[J]. *J Mol Catal(China)*(分子催化), 2014, **28**(2): 157-164.

[3] a. Piumetti M, Hussain M, Fino D, *et al.* Mesoporous silica supported Rh catalysts for high concentration N_2O decomposition[J]. *Appl Catal B: Environ*, 2015, **165**: 158-168.

b. Liu Peng-fei(刘鹏飞), Lou Xiao-rong(娄晓荣), He Kai(何 凯), *et al.* Effects of surfactantson thestructure and catalytic performance of Fe-Mn/ZSM-5/CC monolithic honeycomb catalyst(表面活性剂对 Fe-Mn/ZSM-5/CC 整体式催化剂结构及 NO_x 催化还原性能的影响)[J]. *J Mol Catal(China)*(分子催化), 2014, **28**(3): 227-233.

[4] Lin Y, Meng T, Ma Z. Catalytic decomposition of N_2O over RhO_x supported on metal phosphates[J]. *J Ind Eng Chem*, 2015, **28**: 138-146.

[5] Ates A. Influence of treatment conditions on decomposition activity of N_2O over FeZSM-5 with high iron content[J]. *Catal Sci Technol*, 2014, **4**(7): 2031-2041.

[6] Zou W, Xie P, Hua W M, *et al.* Catalytic decomposition of N_2O over Cu-ZSM-5 nanosheets[J]. *J Mol Catal A: Chem*, 2014, **394**: 83-88.

[7] Xie P, Luo Y J, Ma Z, *et al.* CoZSM-11 catalysts for N_2O decomposition: Effect of preparation methods and nature of active sites[J]. *Appl Catal B: Environ*, 2015, **170/171**: 34-42.

[8] Abu-Zied B M, Soliman S A, Abdellah S E. Enhanced direct N_2O decomposition over $Cu_xCo_{1-x}Co_2O_4$ ($0.0 \leqslant x \leqslant 1.0$) spinel-oxide catalysts[J]. *J Ind Eng Chem*, 2015, **21**: 814-821.

[9] Tursun M, Wang X P, Zhang F F, *et al.* Bi-Co_3O_4 catalyzing N_2O decomposition with strong resistance to CO_2[J]. *Catal Commun*, 2015, **65**: 1-5.

[10] Franken T, Palkovits R. Investigation of potassium doped mixed spinels $Cu_xCo_{3-x}O_4$ as catalysts for an efficient N_2O decomposition in real reaction conditions[J]. *Appl Catal B: Environ*, 2015, **176/177**: 298-305.

[11] Zhang H J, Wang J, Xu X F. Catalytic decomposition of N_2O over $Ni_xCo_{1-x}CoAlO_4$ spinel oxides prepared by sol-gel method[J]. *J Fuel Chem Technol*, 2015, **43**(1): 81-87.

[12] Wang Jian(王 建), Dou Zhe(窦 喆), Pan Yan-fei(潘燕飞), *et al.* Catalytic decomposition of N_2O over $Mn_xCo_{3-x}O_4$ mixed oxides and modified catalysts($Mn_xCo_{3-x}O_4$ 复合氧化物及改性催化剂催化分解 N_2O)[J]. *J Mol Catal (China)*(分子催化), 2015, **29**(3): 246-255.

[13] Xue Li(薛 莉), He Hong(贺 泓). Catalytic decomposition of N_2O over Co-M (M=La, Ce, Fe, Mn, Cu, Cr) composite oxide catalysts (Co-M (M=La, Ce, Fe, Mn, Cu, Cr) 复合金属氧化物催化分解 N_2O)[J]. *Acta Phys - Chim Sin* (物理化学学报), 2007, **23**(5): 664-670.

[14] Xue L, Zhang C B, He H, *et al.* Catalytic decomposition of N_2O over CeO_2 promoted Co_3O_4 spinel catalyst[J]. *Appl Catal B: Environ*, 2007, **75**(3/4): 167-174.

[15] Dziembaj R, Zaitz M M, Rutkowska M, *et al.* Nanostructured Co-Ce-O systems for catalytic decomposition of N_2O[J]. *Catal Today*, 2012, **191**(1): 121-124.

[16] Xue L, He H, Liu C, *et al.* Promotion effects and mechanism of alkali metals and alkaline earth metals on cobalt-cerium composite oxide catalysts for N_2O decomposition[J]. *Environ Sci Technol*, 2009, **43**(3): 890-895.

[17] Zhang J L, Hu H, Xu J, *et al.* N_2O decomposition over K/Na-promoted Mg/Zn-Ce cobalt mixed oxides catalysts[J]. *J Environ Sci*, 2014, **26**(7): 1437-1449.

[18] Muroyama H, Hano S, Eguchi Matsui T. Catalytic soot combustion over CeO_2-based oxides[J]. *Catal Today*, 2010, **153**(3/4): 133-135.

[19] Asano K, Ohnishi C, Iwamoto S, *et al.* Potassium-doped Co_3O_4 catalyst for direction decomposition of N_2O[J]. *Appl Catal B: Environ*, 2008, **78**(3/4): 242-249.

[20] Uetsuka H, Aoyagi K, Yuzaki K, *et al.* Isotopic study of nitrous oxide decomposition on an oxidized Rh catalyst: mechanism of oxygen desorption[J]. *Catal Lett*, 2000,

66(1/2): 87-90.

[21] Tanaka S, Yuzai K, Ito S, *et al.* Mechanism of O_2 desorption during N_2O decomposition on an oxidized Rh/USY catalyst[J]. *J Catal*, 2001, **200**(2): 203-208.

溶胶凝胶法制备 $Ce_xCo_{2-x}AlO_4$ 复合氧化物及其催化分解 N_2O

王 建, 吴藏藏, 郑 丽, 徐秀峰*

(烟台大学 应用催化研究所, 山东 烟台 264005)

摘要: 用柠檬酸-溶胶凝胶法制备了 $Ce_xCo_{2-x}AlO_4$ 系列复合氧化物和 K_2CO_3 改性催化剂, 考察了复合氧化物组成、母液 pH 值、钾负载量对 N_2O 分解催化剂活性的影响, 用 N_2 物理吸附、X 射线衍射(XRD)、扫描电镜(SEM)、H_2 程序升温还原(H_2-TPR)、O_2 程序升温脱附(O_2-TPD)、X 射线光电子能谱(XPS)等方法表征了催化剂结构. 结果表明: 用 Ce 取代 Co_2AlO_4 中部分 Co 制得的 $Ce_xCo_{2-x}AlO_4$ 复合氧化物催化活性有所提高, 其中母液 pH=2、组成为 $Ce_{0.05}Co_{1.95}AlO_4$ 的催化剂活性较高, 该催化剂具有较高的比表面积、较小的晶粒及 Ce-Co 间的协同效应; 进一步研究表明, 由于 K 粒子的电子效应, 使得 0.05 K/$Ce_{0.05}Co_{1.95}AlO_4$ 的催化活性又优于其他催化剂, 有氧气氛中 450 ℃连续反应 50 h, N_2O 分解率达 98.5%.

关键词: N_2O 催化分解; $Ce_xCo_{2-x}AlO_4$ 复合氧化物; 溶胶凝胶法; K 改性催化剂